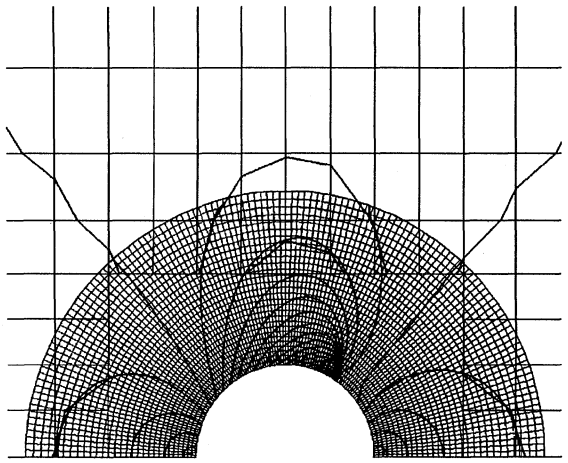

Fig. 6 Mach number contours surrounding the circular cylinder showing minimum chimera-grid overlap and coarse outer-grid conditions, $M_\infty = 0.5$, inner grid = 129 × 31, outer gird = 33 × 17, $R2 = 1.5$, $X1 = 1.0$, and $X2 = 17.5$.

A final solution demonstrating the effects of reduced chimera overlap and a coarse outer grid is displayed in Fig. 6. The inner- and outer-grid dimensions are 129 × 31 and 33 × 17, respectively. Note that the chimera overlap for this case has been significantly reduced. The large disparity in grid spacing at the inner-grid outer boundary is obvious. Nevertheless, the Mach number contours from the two grids in the overlap region are nearly identical to each other. The largest discrepancy in the overlap region arises from the straight-line segments used by the plotting program to represent the contours within each outer-zone grid cell. The solution at the circular cylinder surface, including the shock wave structure, is almost exactly the same as in Fig. 4. The surface pressure coefficient distribution for this case (not shown) is also in excellent agreement with similar results computed using different grid arrangements.

Concluding Remarks

A chimera-based full potential algorithm has been studied using a simple two-dimensional circular cylinder model problem. Both incompressible and shocked-compressible solutions have been used. The results indicate that the multizone chimera grid approach is a viable technique for solving the full potential equation and could provide a very fast computational tool for aerodynamic analysis and design.

A careful study of error produced by the chimera approach was conducted using a two-dimensional, incompressible model problem. A grid refinement study produced nearly identical results from single-zone and two-zone chimera grids, both exhibiting second-order behavior over a wide range of grid refinement. Thus, the additional interpolation-induced error generated by the chimera approach does not affect the basic second-order accuracy of the present numerical scheme.

Numerous chimera-grid arrangements with widely varying overlaps and cell-interface area ratios produced remarkable accuracy (and consistency in accuracy as well) showing little variation in the solutions being studied. In particular, remarkable accuracy at the circular cylinder surface was obtained using an extremely coarse outer grid in the chimera-grid arrangement. These results were produced with the shocked-compressible solution in which a transonic shock wave passed through one of the chimera interface boundaries.

References

[1]Steger, J. L., Dougherty, F. C., and Benek, J. A., "A Chimera Grid Scheme," *Advances in Grid Generation*, edited by K. Ghia and U. Ghia, ASME FED-5, American Society of Mechanical Engineers, New York, 1983, pp. 59–69.

[2]Benek, J. A., Buning, P. G., and Steger, J. L., "A 3-D Grid Embedding Technique," AIAA Paper 85-1523, July 1985.

[3]Buning, P. G., Chan, W. M., Renze, K. J., Sondak, D. L., Chiu, I. T., and Slotnick, J. P., "OVERFLOW User's Manual," Unpublished NASA Rept., Version 1.6ad, March 1993.

[4]Meakin, R., "On the Spatial and Temporal Accuracy of Overset Grid Methods for Moving Body Problems," AIAA Paper 94-1925, June 1994.

[5]Holst, T. L., "Numerical Solution of the Full Potential Equation Using a Chimera Grid Approach," NASA TM-110360, July 1995.

D. S. McRae
Associate Editor

Study of Adaptive Shape Airfoils at Low Reynolds Number in Oscillatory Flows

Wei Shyy,* David A. Jenkins,† and Richard W. Smith‡
University of Florida, Gainesville, Florida 32611

Introduction

MICROAERIAL vehicles (μAVs) with characteristic lengths under 6 in. (15 cm), flight speeds of 20–40 mph (32–64 km/h), and specific payload and endurance needs are potentially useful for many military and civilian applications. The combination of small dimensions and modest flight speed results in Reynolds numbers ranging between 10^4 and 10^5. Traditional rigid airfoil shapes experience substantial degradation in performance (specifically, the lift-to-drag ratio) as the Reynolds number falls through this range. Thus, even ordinary variations in wind speed can cause unwanted changes in behavior. In this study, rudimentary adaptive airfoils, which change their shape in response to changes in velocity, are examined for potential applications in this arena. Candidate designs are first evaluated by the application of detailed computational fluid dynamics simulations in a fluctuating flow. Then, several experimental airfoils are tested in a specially modified wind tunnel to look for corroboration of the predicted effects and other indications of potentially useful behavior.

Theoretical Formulation

A computational methodology has been developed to handle the fluid flow and flexible wing surface structure interaction in the context of a moving boundary problem.[1–3] In addition to solving a set of coupled, nonlinear partial differential equations governing the fluid and structural dynamics, detailed interfacial conditions must be prescribed at the solid–fluid interface at each instant in time. Furthermore, because the location of the solid–fluid interface is not known a priori, the interface position must be computed as part of the overall solution. For this study, the membrane is assumed to be massless with zero thickness and no initial strain. It is considered to be fixed at the leading and trailing edges. The membrane material is assumed to be linearly elastic and in a state of uniaxial stress as it deforms under the aerodynamic loads. The flow is modeled using the Reynolds-averaged Navier–Stokes equations, representing the Reynolds stresses in terms of the mean flow strain rate and an eddy viscosity. The k–ω eddy-viscosity model by Menter[4] is used here.

In the numerical method used, a discrete form of the elastic boundary value problem is obtained at a finite number of points using appropriate second-order accurate finite volume approximations. A pressure-based sequential-implicit algorithm, as described by Shyy,[5] is adopted as the flow solver. The turbulence and membrane equilibrium equations are simply appended to the basic conservation law equation set. All computations are done using time-dependent

Received Dec. 28, 1996; revision received May 1, 1997; accepted for publication May 30, 1997.

*Professor and Chair, Department of Aerospace Engineering, Mechanics and Engineering Science. Associate Fellow AIAA.

†Associate Engineer, Department of Aerospace Engineering, Mechanics and Engineering Science.

‡Postdoctoral Fellow, Department of Aerospace Engineering, Mechanics and Engineering Science; currently Engineer, Naval Surface Weapon Center, Panama City, FL 32407.

body-fitted grids with the membrane imbedded in the center of the computational domain and with the outer boundary located approximately seven chord lengths away. An iterative procedure is used to solve the coupled boundary value problem by computing the elastic and aerodynamic problems cyclically until a converged stationary solution is obtained at every time instant. Details of the present computational algorithm as well as assessment of the numerical accuracy, including a grid dependency test, can be found in Refs. 3 and 6.

For this study, three different airfoil types are analyzed. First, to serve as a basis for comparison, a rigid, circular camber airfoil is selected. Then, an airfoil with a flexible surface, set with an initial circular camber, is used for examination of a simple, purely passive, response. Finally, a hybrid, or tailored passive response, airfoil is used. This airfoil is mathematically constrained to allow increases in camber beyond the preset amount while prohibiting smaller values of camber. The velocity is assumed to fluctuate 30% around the mean value at 1 Hz.

Results of Simulations

Figure 1 shows the variation (at angle of attack = 3 deg, Reynolds number = 7.5×10^4, and Strouhal number = 0.1) in lift coefficient, pitching moment coefficient, and lift-to-drag ratio through one cycle of velocity variation for a 4% circular camber rigid airfoil, a 4% camber flexible airfoil, and a hybrid airfoil limited to 4% camber or greater. Each of the three airfoils shows some sensitivity to the velocity variation, with the flexible airfoil exhibiting the largest swings. Because the separation bubble is still fairly small at this angle of attack, even the rigid shape shows reasonable performance throughout the cycle. The hybrid shape offers no clear advantage under these conditions.

Figure 2 shows the same wings at 7-deg angle of attack. Under these conditions, the separation bubble becomes quite extensive on the rigid shape (see the streamline plots in Ref. 7). The rigid airfoil shows consistently poor lift to drag performance and little sensitivity to variations in velocity throughout the cycle. The flexible wing, on the other hand, is quite responsive to the velocity and shows improvements in lift to drag during the accelerated portion of the flow, with some degradation during the slower portion. The streamline plots for this case show that flow separation is largely confined to the leading-edge region most of the time, probably because of the spontaneous changes in shape of the flexible membrane. By stopping the camber at 4%, the hybrid wing seems to effectively limit the degradation in performance while retaining the favorable behavior, resulting in an obvious net improvement.

These simulations are not limiting cycle cases; rather, they represent the state of affairs shortly after the oscillating flow begins. The simulations of the flexible airfoils should not be confused with a simple series of rigid, circular camber airfoils subjected to different, fixed velocities. First, the computed airfoil shape is not circular at any given instant. Instead, the shape responds in some way (appropriately or not) to the instantaneous pressure distribution developed. Second, the flow solution and the elastic solution at each time instant depend on the starting conditions presented by the previous solutions at the previous time instant. The passive response of the flexible membrane used here is obviously a very crude form of adaptation, but it at least represents a useful first step and one that can be verified experimentally.

Experimental Program

To provide a fluctuating freestream velocity environment for the experimental studies, a low-turbulence, 3 × 3 ft wind tunnel was modified by adding a flow modulating device similar to that suggested by Al-Asmi and Castro.[8] In this case, the flow restrictor is placed at the exhaust of the open circuit tunnel, as shown schematically in Fig. 3. Depending on the mean velocity in the tunnel and the speed of rotation, the velocity can be modulated by up to 25%. The variation in velocity was found to be approximately sinusoidal, with some improvements expected in the future by slight trimming of the shape of the openings. The turbulence in the test section with no modulation was measured at 0.04% using a hot-wire anemometer.

Because a two-dimensional study was required, vertically oriented splitter plates were added to the test section. The test airfoils,

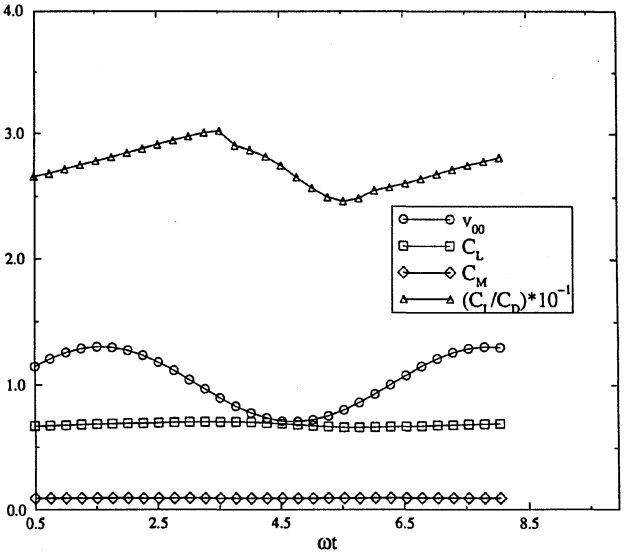

a) Rigid

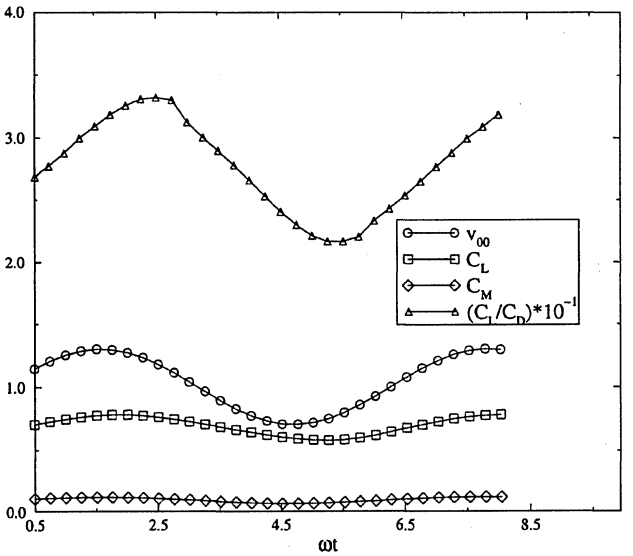

b) Flexible

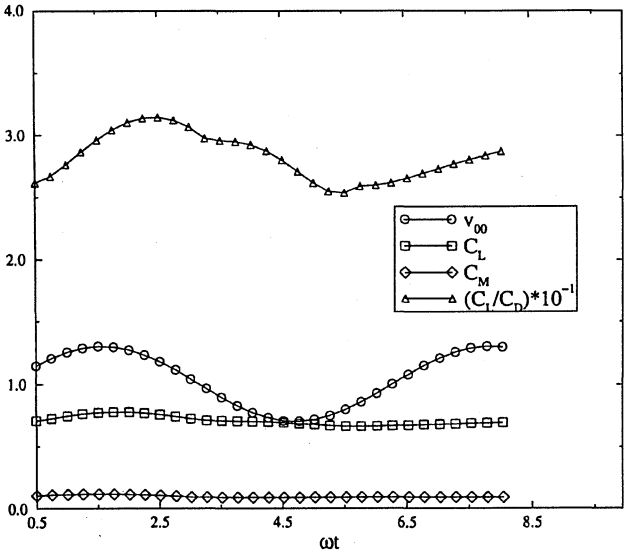

c) Hybrid

Fig. 1 Time series for 4% camber circular arc airfoils, $Re = 7.5 \times 10^4$, $Sr = 0.10$, and angle of attack = 3 deg.

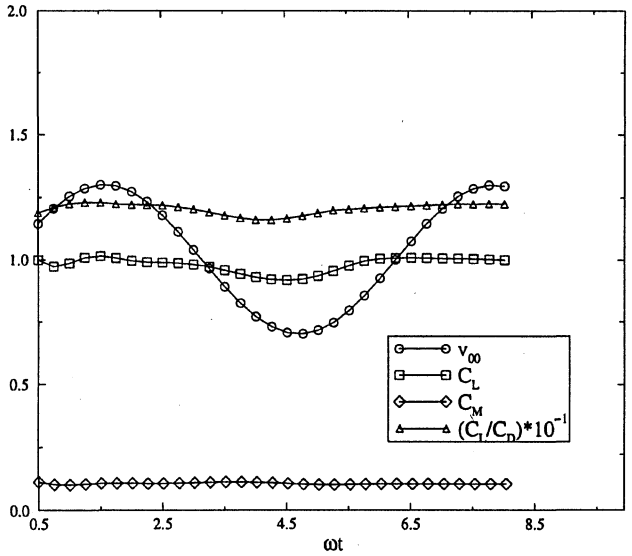

a) Rigid

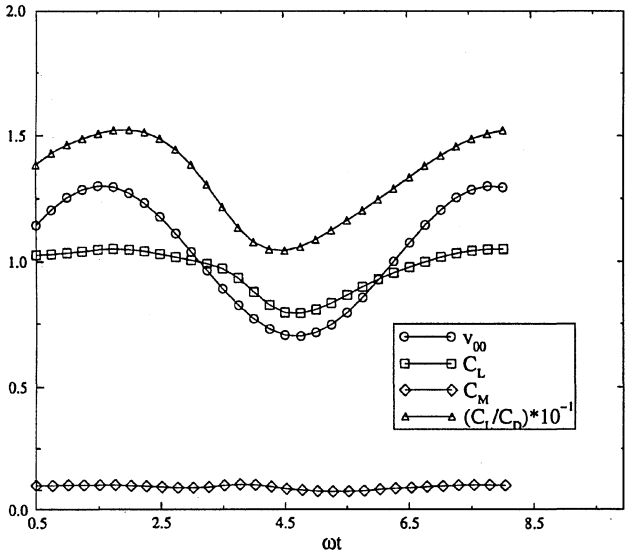

b) Flexible

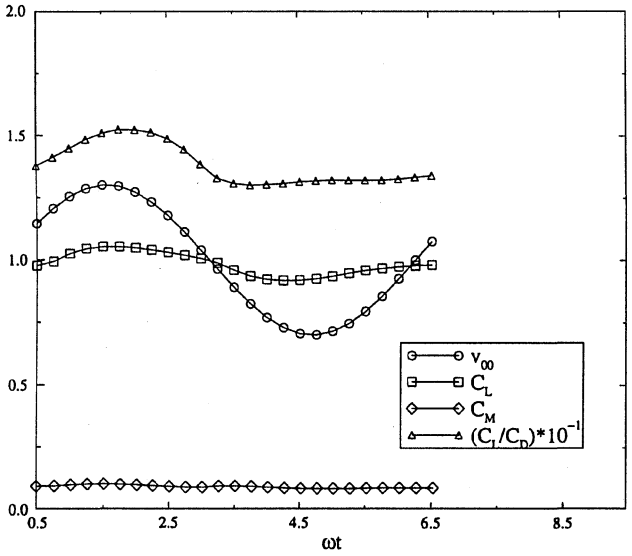

c) Hybrid

Fig. 2 Time series for 4% camber circular arc airfoils, $Re = 7.5 \times 10^4$, $Sr = 0.10$, and angle of attack = 7 deg.

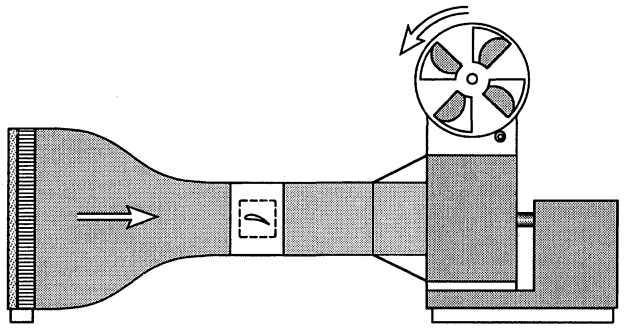

Fig. 3 Oscillating-flow wind tunnel used in the experimental study, showing the flow-restricting device on the exhaust.

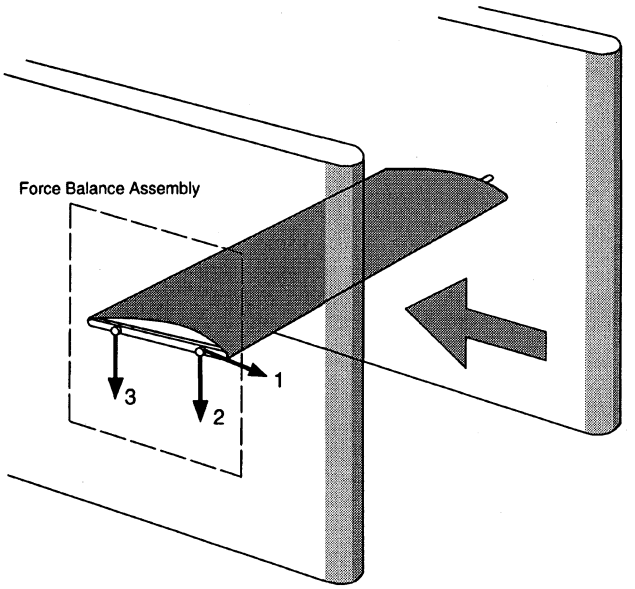

Fig. 4 Test airfoil support system; force measurement links 1, 2, and 3 are used to make dynamic measurements of lift, drag, and pitching moment.

which are 12 in. long with a 4-in. chord, are supported horizontally between the splitter plates. The test airfoil frames were fabricated by welding together lengths of $\frac{1}{8}$-in.-diam steel rod and square stock. Flexible membrane wings were made by gluing a sheet of 0.004-in. latex rubber to the frame, with very little prestretch. For the rigid shapes desired, 0.020-in.-thick fiberglass sheets were glued to the prepared top surface of the frame after removing a commensurate amount of material. In this way, the shapes of all of the test wings were kept as similar as possible so that meaningful comparisons could be made. The hybrid airfoil was difficult to emulate experimentally. It was finally approximated by placing a curved wire screen beneath the flat flexible membrane. With some trial and error, an initial curvature (close to 6% camber) was found that allowed the membrane to lift free of the screen for about half of the cycle and then be constrained by the screen for the next half cycle. Dynamic measurements of the very small lift and drag forces required the fabrication of a sensitive force measurement system, which utilized thin beam load cells connected to three links at two of the airfoil support points. Data were digitally recorded at 2-kHz sampling rate on each of the three channels. Figure 4 shows the arrangement of the support and measurement components.

Results of Experiments

The first series of experiments, which is reported here, was conducted at a mean freestream velocity of 35.4 fps, resulting in an average Reynolds number of 7.5×10^4, chosen to be the same as in the numerical study. The modulation frequency was set at 1.7 Hz to achieve a Strouhal number of 0.1, as in the simulations. At this velocity, the variation caused by the flow modulator was about 10%. The angle of attack was fixed at 7 deg for all of the tests. An initially flat flexible membrane wing was observed to assume an

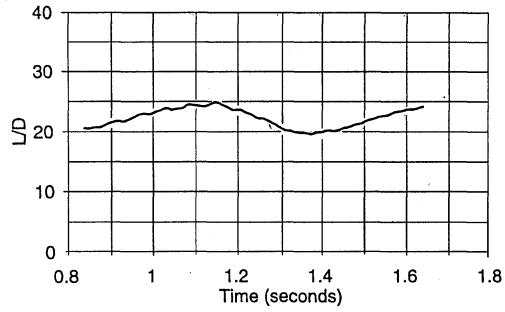

a) Six-percent camber rigid wing

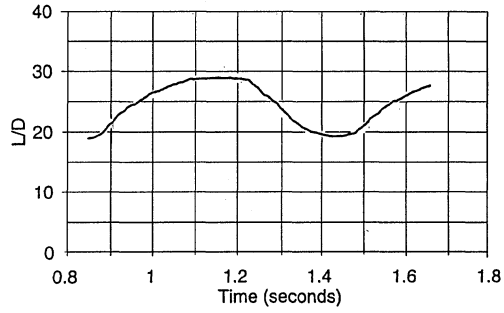

b) Latex membrane wing, which exhibits about 6% camber at 35.4 fps

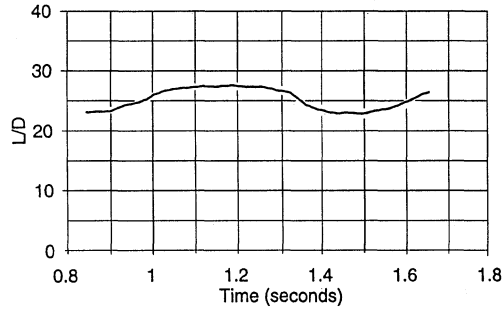

c) Hybrid wing with curved wire screen camber stop

Fig. 5 Experimental time series at $Re = 7.5 \times 10^4$, $Sr = 0.10$, and angle of attack = 7 deg.

approximate 6% camber at this mean velocity, and so the results can be reasonably compared with the simulation flexible airfoil with an initial camber value. Because many hundreds of cycles take place before the data are recorded, this is a limiting cycle case, unlike the case examined in the numerical simulations.

Figure 5 shows measured lift-to-drag ratios throughout one complete cycle for the three test airfoils described. The 6% camber rigid wing (shown in Fig. 5a) exhibits a mild sensitivity to the velocity variation. The membrane covered flat wing, which was observed to fluctuate around approximately 6% camber, is shown in Fig. 5b. Substantial variation in the lift-to-drag ratio is observed, consistent with what would be expected with the observed changes in camber as the velocity changes. The lift-to-drag ratio is improved during the accelerating part of the cycle; however, some degradation in performance occurs during the decelerating portion. Finally, the hybrid wing with the curved screen insert gives the results shown in Fig. 5c. The sensitivity to velocity variation is smaller than that of the pure flexible wing, and yet the overall performance is higher.

Conclusions

The focus of the present study is on the aerodynamic performance of the μAV in low Reynolds number unsteady flows. Each of the experimental wings showed behavior qualitatively similar to that shown in their numerical simulation counterparts, even though the shapes and construction features were not exactly the same, as mentioned. The hybrid wing in particular demonstrated that it is possible to combine improvements during accelerating flows with sustained performance during deceleration. It seems likely that, by using more aggressive and more active adaptation strategies than the very simple ones presented here, practical μAV wings with improved performance qualities can be realized.

Acknowledgments

The present effort has been sponsored in part by a grant from The Boeing Company. We are grateful for the contributions of Richard Fearn and Thomas Marin in the experimental setup.

References

[1]Smith, R. W., and Shyy, W., "Computation of Unsteady Laminar Flow over a Flexible Two-Dimensional Membrane Wing," *Physics of Fluids*, Vol. 7, No. 8, 1995, pp. 2175–2184.

[2]Smith, R., and Shyy, W., "Computational Model of Flexible Membrane Wings in Steady Laminar Flow," *AIAA Journal*, Vol. 33, No. 10, 1995, pp. 1769–1777.

[3]Shyy, W., Udaykumar, H. S., Rao, M. M., and Smith, R. W., *Computational Fluid Dynamics with Moving Boundaries*, Taylor and Francis, Washington, DC, 1996, Chap. 3.

[4]Menter, F. R., "Two-Equation Eddy-Viscosity Turbulence Models for Engineering Applications," *AIAA Journal*, Vol. 32, No. 8, 1994, pp. 1598–1605.

[5]Shyy, W., *Computational Modeling for Fluid Flow and Interfacial Transport*, Elsevier, Amsterdam, 1994, Chap. 5.

[6]Smith, R. W., and Shyy, W., "Computation of Aerodynamic Coefficients for a Flexible Membrane Airfoil in Turbulent Flow: A Comparison with Classical Theory," *Physics of Fluids*, Vol. 8, No. 12, 1996, pp. 3346–3353.

[7]Shyy, W., and Smith, R. W., "A Study of Flexible Airfoil Aerodynamics with Application to Micro Aerial Vehicles," AIAA Paper 97-1933, June 1997.

[8]Al-Asmi, K., and Castro, I. P., "Production of Oscillatory Flow in Wind Tunnels," *Experiments in Fluids*, Vol. 15, Jan. 1993, pp. 33–41.

A. Plotkin
Associate Editor

Improvements to a Dual-Time-Stepping Method for Computing Unsteady Flows

S. DeRango* and D. W. Zingg†
University of Toronto,
Downsview, Ontario M3H 5T6, Canada

Introduction

IMPLICIT time-marching methods are preferred for computing many unsteady aerodynamic flows because of physical and numerical stiffness. However, a fully implicit method can be expensive because the solution of a nonlinear problem is required at each time step. The approximately factored algorithm of Beam and Warming with local time linearization[1] is an efficient option, capable of retaining both second-order accuracy in time and unconditional stability. In practice, first-order time accuracy is often obtained as a result of approximate linearization of the artificial dissipation and turbulence models, low-order treatment of boundary and interface conditions, and loose coupling of a field-equation turbulence model. An alternative approach, which has become popular in recent years, is to apply an algorithm developed for steady flows to the nonlinear problem arising at each iteration of the implicit time-marching method.[2–8] Thus one can apply an algorithm with non-time-accurate convergence acceleration techniques such as local preconditioning, local time stepping, diagonalization, and multigrid. Such methods are typically called dual-time-stepping or subiteration methods.

Received June 12, 1996; presented as Paper 96-2088 at the AIAA 2nd Fluid Dynamics Conference, New Orleans, LA, June 17–20, 1996; revision received April 21, 1997; accepted for publication April 30, 1997.

*Graduate Student, Institute for Aerospace Studies, 4925 Dufferin Street.

†Associate Professor, Institute for Aerospace Studies, 4925 Dufferin Street. Member AIAA.